Nonlinear Aerodynamic Reduced-Order Model for Limit Cycle Oscillation and Flutter

Weiwei Zhang*, Jiaqing Kou†, Ziyi Wang‡

Northwestern Polytechnical University, Xi'an 710072, People's Republic of China

*(Manuscript accepted by **AIAA Journal**)*

DOI: 10.2514/1.J054951

Nomenclature

a	=	location of the pitching axis
a_∞	=	speed of sound
b	=	half-chord length
$\boldsymbol{C}$	=	correlation matrix of proper orthogonal decomposition
C_l	=	lift coefficients
C_m	=	pitch moment coefficients
c	=	mean aerodynamic chord
$\boldsymbol{D}$	=	column matrix of eigenvectors of $\boldsymbol{C}$
DT	=	non-dimensionalized time step of aerodynamic time-marching
$\boldsymbol{d}_1$	=	eigenvector of $\boldsymbol{C}$ with the biggest eigenvalue
dt	=	physical time step
H	=	complex-conjugate-transpose of a matrix
h	=	plunge displacement of an airfoil
h_{LCO}	=	maximum plunging amplitude of a limit cycle oscillation response
$\boldsymbol{I}$	=	identity matrix
k	=	reduced frequency
M	=	Mach number

* Professor, School of Aeronautics, National Key Laboratory of Aerodynamic Design and Research; aeroelastic@nwpu.edu.cn (Corresponding Author)
† Graduate Student, School of Aeronautics, National Key Laboratory of Aerodynamic Design and Research; koujiaqing93@163.com
‡ Graduate Student, School of Aeronautics, National Key Laboratory of Aerodynamic Design and Research; jet_boy@126.com

p = number of sample in a segment of training case

q = number of radial basis function in the hidden layer

r = relative error of ROM predictions and CFD simulations

r_α = gyration radius of the airfoil around the elastic axis

St = Strouhal number

$\boldsymbol{T}$ = output matrix of the hidden layer

T_∞ = freestream temperature

t = current time instant

$\boldsymbol{U}$ = left singular matrix of $\boldsymbol{T}$

$\boldsymbol{V}$ = right singular matrix of $\boldsymbol{T}$

V^* = reduced velocity

$\boldsymbol{v}_j$ = center vector of the jth hidden neuron

$\boldsymbol{W}$ = weight matrix of the output layer

$\boldsymbol{X}_j$ = the jth segment of training case

$\boldsymbol{x}_i$ = the jth training sample

x_α = airfoil static unbalance value

$\boldsymbol{Y}$ = output matrix of radial basis function neural network

$\boldsymbol{y}_{ROM}$ = outputs from CFD data

$\boldsymbol{y}_{CFD}$ = outputs from reduced-order model

$\boldsymbol{\Lambda}$ = diagonal matrix of eigenvalues of $\boldsymbol{C}$

α = pitch angle of an airfoil

α_0 = mean angle of attack of pitching motion

α_{LCO} = maximum pitching amplitude of a limit cycle oscillation response

μ = mass ratio

$\boldsymbol{\Sigma}$ = diagonal matrix with singular value of $\boldsymbol{G}$ on its main diagonal

$\boldsymbol{\sigma}$ = width matrix of the hidden layer

ω_α = uncoupled natural frequency of pitch

ω_h = uncoupled natural frequency of plunge

Ⅰ. Introduction

Aeroelasticity focuses on the interaction between unsteady flow field and flexible structure. Among current studies in aeroelastic systems, nonlinear behavior is gaining more and more concentration [1]. In aeroelastic systems, both the aerodynamic forces and structural responses exhibit nonlinear effects. Shock waves, viscous effects and separated flows in aerodynamic flows account for the aerodynamic nonlinearities, whereas control surface freeplay and geometric structural nonlinearities always induce structural nonlinearities. As a typical phenomenon which only occurs in nonlinear systems, limit cycle oscillation (LCO) beyond the flutter boundary is a nonlinear behavior dominated by dynamic nonlinearity, even though not all nonlinear systems exhibit this characteristic. LCO may appear when either or both the structural and aerodynamic models are dynamically nonlinear. In this Note, transonic aerodynamic nonlinearities are introduced for observing the nonlinear LCO behaviors, with a dynamically linear structure considered.

Currently, numerical simulation is one of the popular methods in studying the mechanisms of aeroelastic systems [2-3]. By means of high-fidelity computational fluid dynamics (CFD) solver, the complex phenomena in unsteady flow can be precisely described. However, the high computational cost of CFD technique makes such investigations very inconvenient in engineering applications. To overcome this limitation, many reduced-order models (ROMs) have been proposed. There are two groups of ROMs utilized in aeroelasicity [4]: the first is the group of methods based on the extraction of flow characteristics, including proper orthogonal decomposition (POD), which projects the flow snapshots into several dominant low-order vector bases [5]. The second branch exploits the system

identification methods to build the relationship between input and output data. Linear models, such as autoregressive with exogenous input (ARX) model [6-7], or nonlinear models, like radial basis function (RBF) neural network [8] and other neural networks [9], have been widely used in predicting nonlinear aerodynamic responses. Recently, some combinations between linear and nonlinear models [10] or combinations between POD and system identification methods [11] have been proposed.

In aeroelastic modeling field, a great many of reduced-order modeling methods including aerodynamic describing functions [12], neural networks [8-9] and Volterra series [13] are utilized in order to simulate the nonlinear dynamics due to the fluid-structure interaction. For example, Zhang et al. [8] introduced a kind of recursive radial basis function (RRBF) neural network and predicted the LCO behavior of a NACA 64A010 airfoil. However, most of these studies did not consider the responses after the variations of structural parameters, since the change of structural parameters may lead to large variations of the LCO velocity and frequency, which poses a big challenge on the generalization capability of nonlinear aerodynamic ROMs.

In this study, some improvements are proposed based on the RRBF network model given by Zhang et al. [8], while permitting relatively accurate LCO predictions after structural parameters change. In current reduced-order modeling practice, both width determination introduced by Kou and Zhang [14] and center selection via POD technique proposed by Zhang et al.[15] are combined for better modeling the previous RRBF neural network aerodynamic model. This new ROM is named as a POD-RBF network. The constructed POD-RBF network is applied to predict unsteady aerodynamic forces of a NACA64A010 airfoil. After coupling with structural equations of motion, the LCO trends and bifurcation point under different structural parameters can be predicted within a fraction of time. Comparisons with simulations from nonlinear RRBF network and linear ARX model indicate that

wider potential applications in nonlinear aeroelasticity can be exploited from the proposed ROM based on a POD-RBF network.

Ⅱ. Reduced-Order Modeling

A. RRBF Neural Network

RBF neural network is a classical three-layered feedforward neural network, with a cascade structure including input, hidden and output layers [16]. RBFs are used as the hidden neurons, producing nonlinear mappings of the input vector. The outputs of the hidden layer are linearly weighted in order to calculate the final outputs. When output feedback is introduced, a RRBF neural network described in [8] is constructed.

B. Parameter Selection of Nonlinear ROM

Although RBF neural network is good at learning mappings from input-output data, the overfitting caused by redundant samples is still a tough problem among current modeling practices. Width matrix σ, number of hidden layer neurons q, center vector $\boldsymbol{v}_j$ of each RBF and weight matrix $\boldsymbol{W}$ of the output layer are all undetermined parameters that need effective learning. Recently, Zhang et al. [15] proposed a center selection technique by POD, which enhanced the performance of RBF network in time series prediction. Kou and Zhang [14] introduced a validation case and utilized particle swarm optimization (PSO) algorithm for determining the best width matrix. In this Note, these two approaches are both adopted. After the widths and centers are decided, singular value decomposition (SVD) is utilized for calculating the output weight matrix.

C. Modeling by the POD-RBF Network

The process of constructing the proposed POD-RBF network is shown in this section. Firstly, the training case and validation case are calculated by CFD solver. Then the centers are decided by POD as

follow:

1) Set the sample interval l for choosing a center;

2) According to the interval, separate the training case into q segments with p samples in one segment. The correlation matrix of the jth segment $\boldsymbol{X}_j = \left[\boldsymbol{x}_{l\times p+1}, ..., \boldsymbol{x}_{l\times(p+1)} \right]$ is given by

$$\boldsymbol{C} = \boldsymbol{X}_j{}^T \boldsymbol{X}_j \tag{1}$$

3) Calculate the eigenvalues and eigenvectors of matrix $\boldsymbol{C}$, where $\boldsymbol{D}$ is the column matrix of eigenvectors and $\boldsymbol{\Lambda}$ is the diagonal matrix of eigenvalues:

$$\boldsymbol{CD} = \boldsymbol{D\Lambda} \tag{2}$$

4) Arrange the eigenvalues of $\boldsymbol{C}$ in descending order, and choose the eigenvector $\boldsymbol{d}_1$ with the biggest eigenvalue;

5) The current segment of training case is projected onto the eigenvector $\boldsymbol{d}_1$ and normalized by the Frobenius norm of $\boldsymbol{d}_1$. Then we get the center vector $\boldsymbol{v}_j$ of the jth hidden neuron:

$$\boldsymbol{v}_j = \frac{(\boldsymbol{X}_j \boldsymbol{d}_1)}{\| \boldsymbol{d}_1 \|_F^2} \tag{3}$$

By applying the above process for every segment of the training case, the center of each hidden neuron will be settled. In the third step, the width matrix is given by a particle of PSO, and the weight matrix can be calculated subsequently. The output matrix $\boldsymbol{Y}$ is the product of hidden output matrix $\boldsymbol{T}$ and weight matrix $\boldsymbol{W}$:

$$\boldsymbol{Y} = \boldsymbol{WT} \tag{4}$$

In case of numerical instability, QR decomposition, pseudo inverse method and SVD can be chosen as the pre-processing of matrix $\boldsymbol{T}$. Here we adopt SVD:

$$\boldsymbol{T} = \boldsymbol{U\Sigma V}^{\mathrm{H}}, \boldsymbol{U}^{\mathrm{H}}\boldsymbol{U} = \boldsymbol{I}, \boldsymbol{V}^{\mathrm{H}}\boldsymbol{V} = \boldsymbol{I} \tag{5}$$

$$\boldsymbol{T}^{-1} = \boldsymbol{V\Sigma U}^{\mathrm{H}} \tag{6}$$

$$\boldsymbol{W} = \boldsymbol{Y}\boldsymbol{T}^{-1} = \boldsymbol{Y}\boldsymbol{V}\boldsymbol{\Sigma}\boldsymbol{U}^{\mathrm{H}} \tag{7}$$

where $\boldsymbol{U}$, $\boldsymbol{V}$ are left and right singular matrix of $\boldsymbol{T}$, $\boldsymbol{I}$ is a identity matrix, and $\boldsymbol{\Sigma}$ is a diagonal matrix with singular value of $\boldsymbol{T}$ on its main diagonal. Now the problems of parameter selection are properly addressed.

When a POD-RBF network is obtained, the fitness function of PSO is calculated. If the terminal condition (e.g., preset error bound or number of iterations) is reached, the POD-RBF network is obtained. Otherwise, the user should turn back to the third step for another width matrix until the terminal condition is satisfied. Note that the width optimization by PSO takes the main amount of time in training the proposed ROM, which accounts for the extra time cost compared with the previous RRBF model. The resulting POD-RBF network can be coupled with structural equations of motion for aeroelastic simulations or directly used for aerodynamic predictions under different amplitudes and frequencies.

Ⅲ. Time Marching Method of the Aeroelastic System

A Euler-equation-based unsteady flow solver has been applied for this investigation. Although viscous effects are ignored, adopting the Euler flow model will enhance the resulting LCOs by the large movements of shock waves over the airfoil [9]. Spatial discretization is accomplished by a cell-centered finite volume formulation using a center-differencing scheme. The governing equations are non-dimensionalized by the mean aerodynamic chord *c*, speed of sound a_∞, and freestream temperature T_∞. Further details of numerical methods can be found in [17]. The computational grid deformation scheme is based on RBF interpolation [18]. Our CFD solver has been tested in some cases like flutter or buffet phenomenon [2-3]. The fourth-order accuracy hybrid linear multi-step method [19] is used to solve the aeroelastic equation in the time domain. Other details about the linear structural

model and parameters are described in [8]. The aerodynamic time step *DT* is non-dimensionalized by $DT = dt / (2 \cdot b / a_\infty)$, where *dt* is the physical time step.

Ⅳ. Results and Discussion

A NACA64A010 airfoil pitching and plunging at Mach 0.8 is studied both in aerodynamic modeling and aeroelastic simulations. In order to access the proposed POD-RBF network, the previous RRBF neural network in [8] is adopted for comparison. The two ROMs are trained by the same training case. Furthermore, LCO trends under variations of structural parameters and comparisons of flutter characteristics are given.

A. Training Case

The aerodynamic time step *DT* is fixed to 1 and 0.4 for each ROM and CFD simulations, respectively. The delay orders of two ROMs are both 2 for input and 3 for output. Lift and moment coefficients are modeled together, constructing a multi-input/multi-output (MIMO) system. A training case is designed as a weighted and smoothed random signal filtered within prescribed frequency band. This signal is shown in Fig. 1a. Besides training case, a validation case under small amplitudes is provided for width determination [14] shown in Fig. 1b. In this study, each center is chosen from every 60 consecutive samples, resulting in a low-complexity neural network with 50 centers. The frequency spectrum through fast Fourier transformation is shown in Fig. 2.

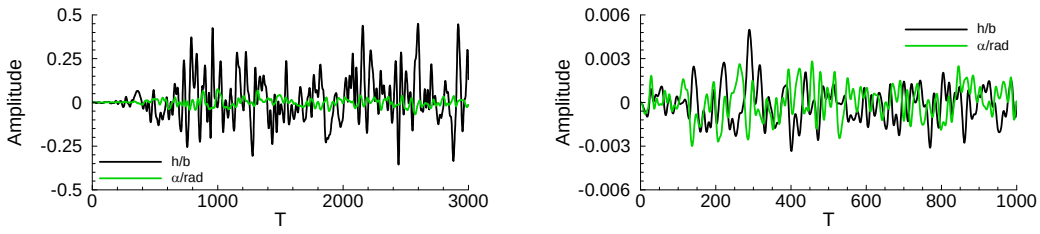

a) **b)**

Fig. 1 Training and validation inputs: a) Training inputs with 3000 time steps, b) Validation inputs with 1000 time steps.

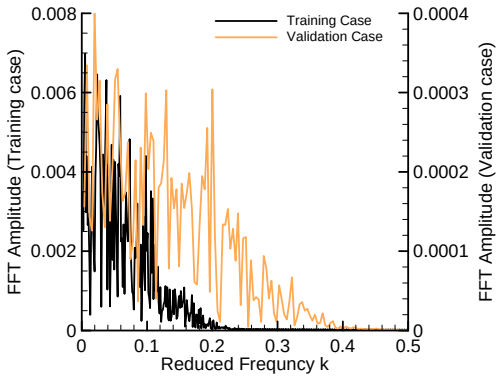

Fig. 2 Fourier analysis of training and validation cases, both in pitching degree of freedom.

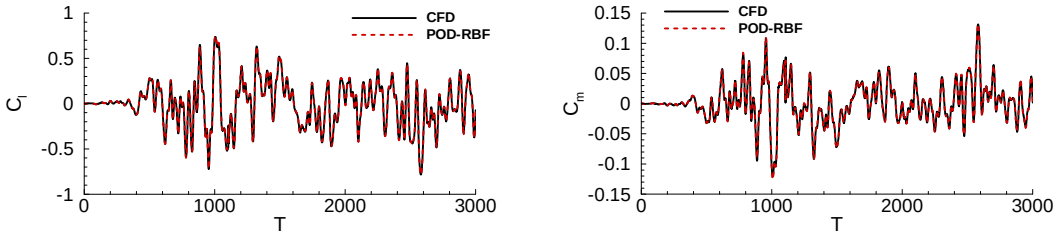

a) **b)**

Fig. 3 Identification of training case: a) Lift coefficient, b) Moment coefficient.

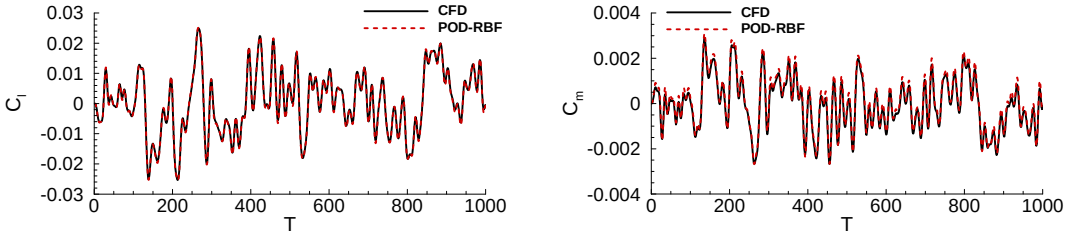

a) **b)**

Fig. 4 Identification of validation case: a) Lift coefficient, b) Moment coefficient.

B. Modeling Unsteady Aerodynamics

Figs. 3-4 demonstrate the identification results of training and validation cases. Relative error is used to estimate the accuracy, defined by Eq. (8):

$$r = \frac{\left\| \boldsymbol{y}_{ROM} - \boldsymbol{y}_{CFD} \right\|_F^2}{\left\| \boldsymbol{y}_{CFD} \right\|_F^2} \times 100\% \quad (8)$$

where $\boldsymbol{y}_{ROM}$ is the prediction of ROM and $\boldsymbol{y}_{CFD}$ is the result given by CFD simulations. For lift coefficients, relative errors of training and validation cases are 2.90% and 4.11% respectively, whereas for pitching moment the errors are 3.96% and 14.62%. Because of limited training samples under small amplitudes and stronger nonlinear dynamics existed in moment, predictions of moment coefficient are

not as good as the lift.

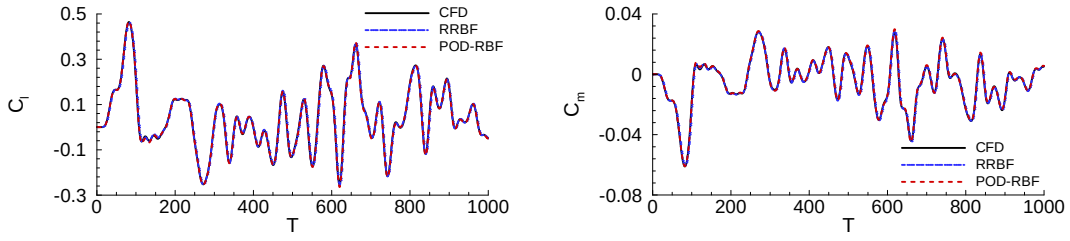

Fig. 5 Comparison of a random pitching motion (case 1): a) Lift coefficient, b) Moment coefficient.

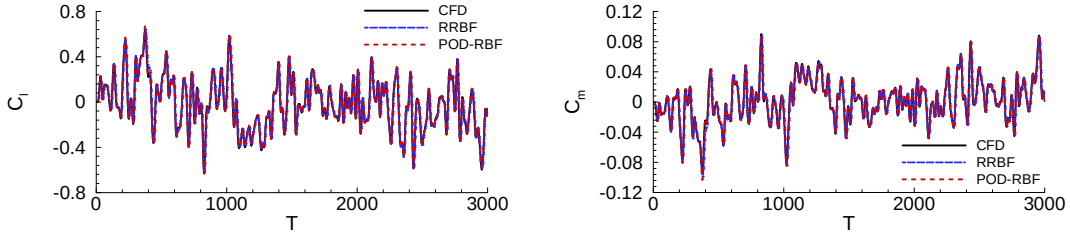

Fig. 6 Comparison of random motions both in pitching and plunging DOFs (case 2): a) Lift coefficient, b) Moment coefficient.

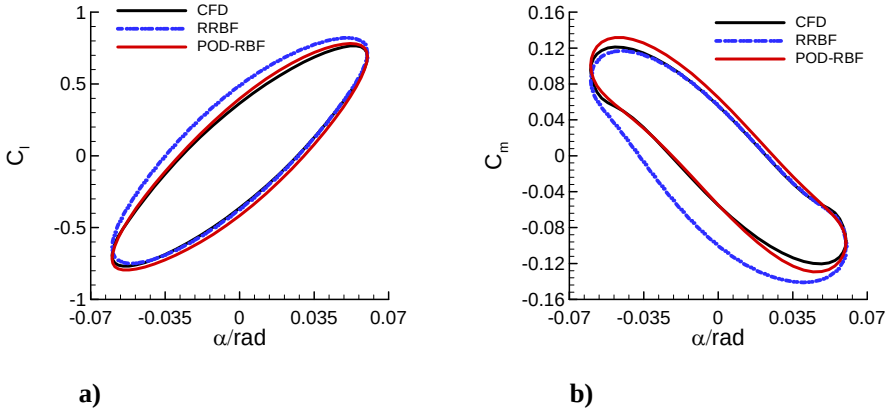

Fig. 7 Predictions of harmonic motions at *St*=0.0125: a) Lift coefficient, b) Moment coefficient.

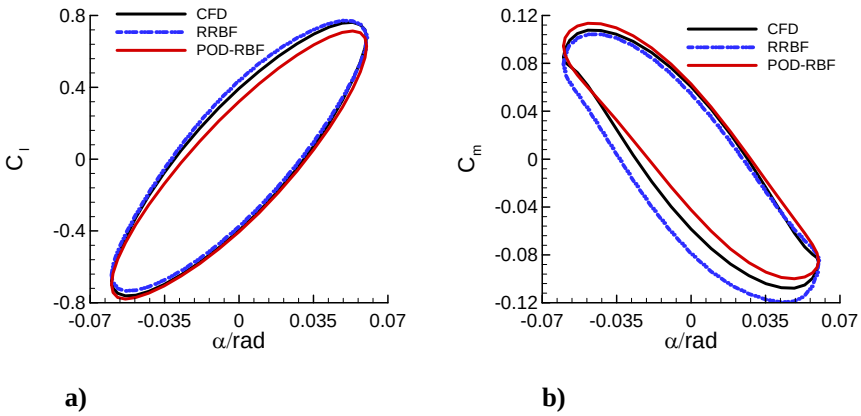

Fig. 8 Predictions of harmonic motions at *St*=0.0225: a) Lift coefficient, b) Moment coefficient.

The performance of unsteady aerodynamic modeling is evaluated by three types of test cases. Figs. 5-6 are identified results of random motions with only pitching degree of freedom (DOF) and both pitching and plunging DOFs, where ideal accuracy can be obtained by both ROMs. Figs. 7-8 show the outputs of harmonic motions with 2 DOFs, under two Strouhal number: St = 0.0125 and St = 0.0225, respectively. The comparison of relative errors is shown in Table. 1. The POD-RBF network outperforms the RRBF model in most of cases, indicating a better overall performance in unsteady aerodynamic modeling.

Table 1 Relative error comparison of four test cases

Case	C_l of POD-RBF	C_l of RRBF	C_m of POD-RBF	C_m of RRBF
Case 1	2.92%	1.90%	3.72%	2.20%
Case 2	3.69%	2.73%	4.77%	3.63%
Case 3	4.89%	10.34%	7.51%	18.98%
Case 4	7.38%	4.70%	9.58%	12.82%

C. LCO Trend and Flutter Characteristics

The standard flow and structural parameters are taken from [20] (i.e., M=0.8, $\alpha_0 = 0^\circ$, a = -0.6, $x_\alpha = 0.25$, $r_\alpha{}^2 = 0.75$, $\omega_h / \omega_\alpha = 0.5$ and $\mu = 75$), and LCO trends under different structural parameters (e.g., frequency ratio and mass ratio) are also simulated. Furthermore, comparisons of the bifurcation point at different structural parameters are provided in comparison with flutter characteristics obtained by ARX model [6-7].

Fig. 9 shows the calculated LCO trends under standard conditions by CFD time marching method. Results are compared with harmonic balance [20] and other CFD solvers [8, 9, 12]. From Fig. 9, a good agreement is presented. In Fig. 10, LCO trends according to amplitudes are displayed. Although both bifurcation velocity and frequency ratio are well captured by the two models, RRBF model performs worse as V^* increases.

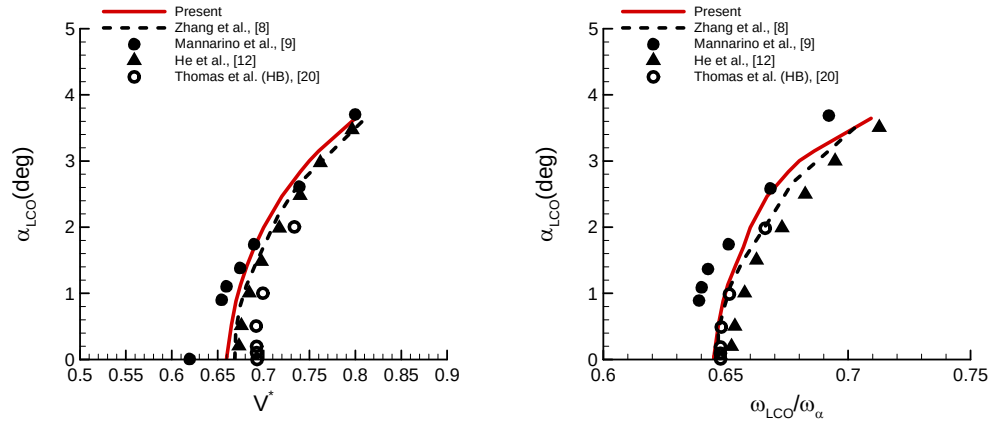

a) **b)**

Fig. 9 Comparison of LCO behaviors of a NACA64A010 airfoil with previous studies: a) LCO velocity, b) LCO frequency.

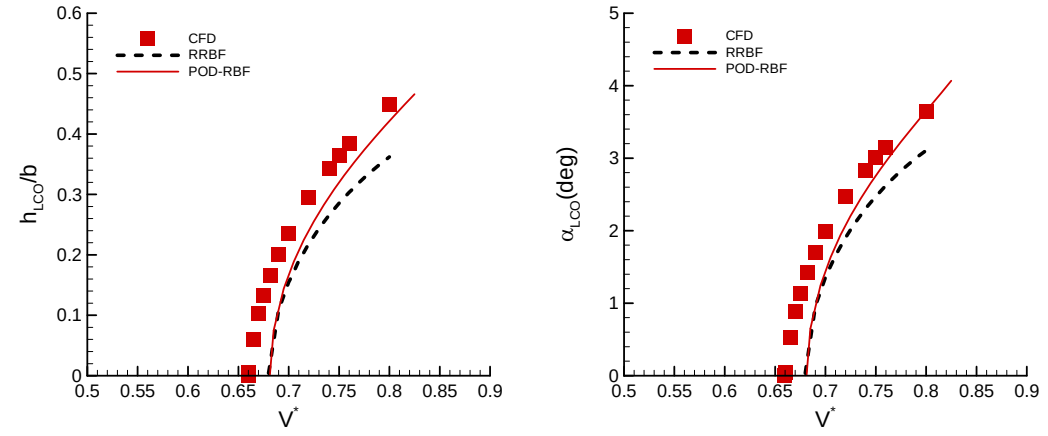

a)

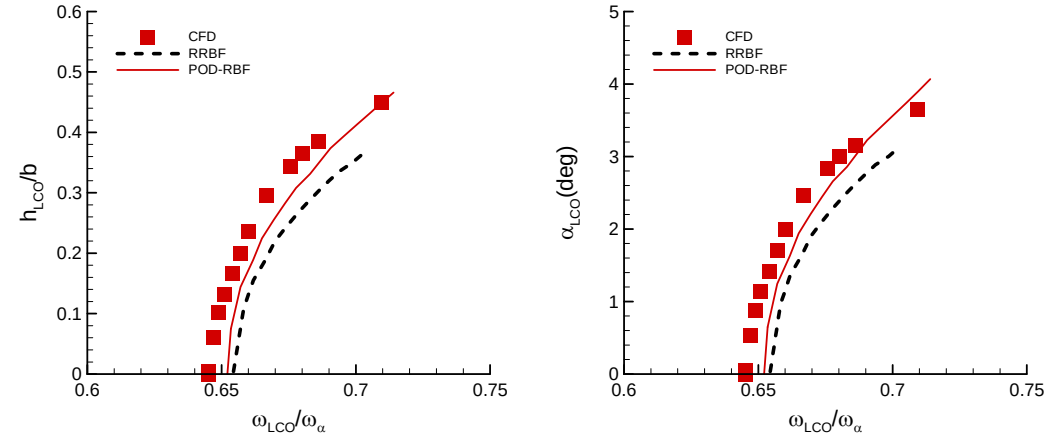

b)

Fig. 10 Compared LCO trends of a NACA64A010 airfoil: a) LCO velocity, b) LCO frequency

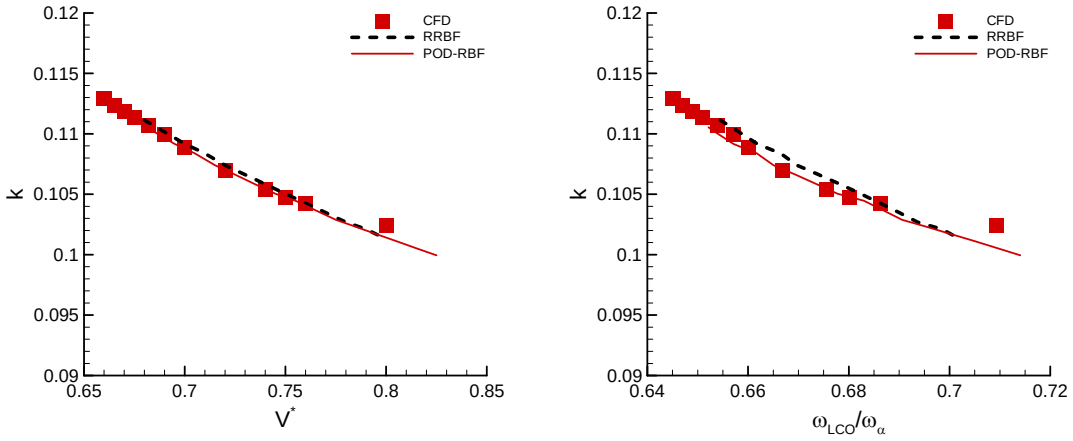

a) **b)**

Fig. 11 Comparison of LCO frequency trends: a) LCO reduced frequency changes with velocity, b) LCO reduced frequency changes with frequency.

Furthermore, trends of LCO varying with reduced frequency *k* are also given in Fig. 11, where better agreement is given by the POD-RBF network model. Fig. 12 shows the LCO behaviors at reduced velocities $V^* = 0.76$ and $V^* = 0.8$. The results of nonlinear POD-RBF network agree well with those calculated by CFD solver, but RRBF model has larger deviations in amplitudes and phase differences.

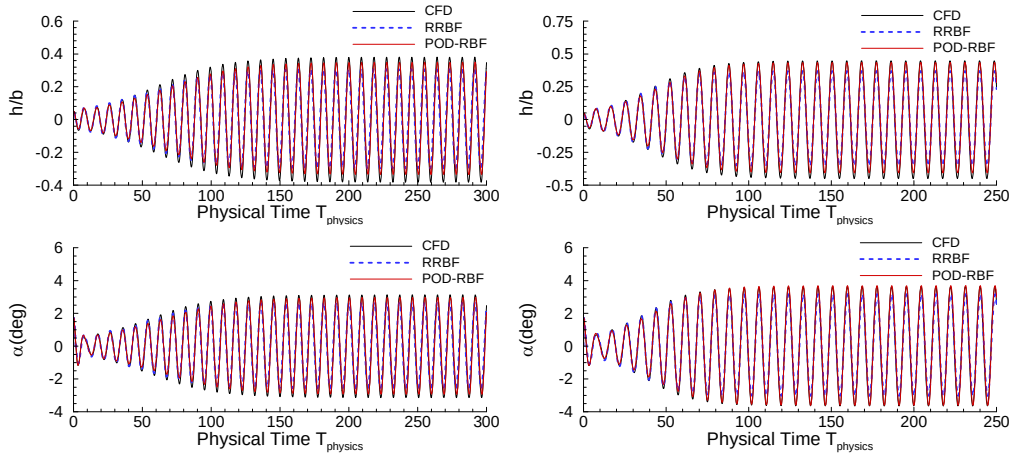

a) **b)**

Fig. 12 LCO responses at two different reduced velocities: a) $V^* = 0.76$ **, b)** $V^* = 0.8$**.**

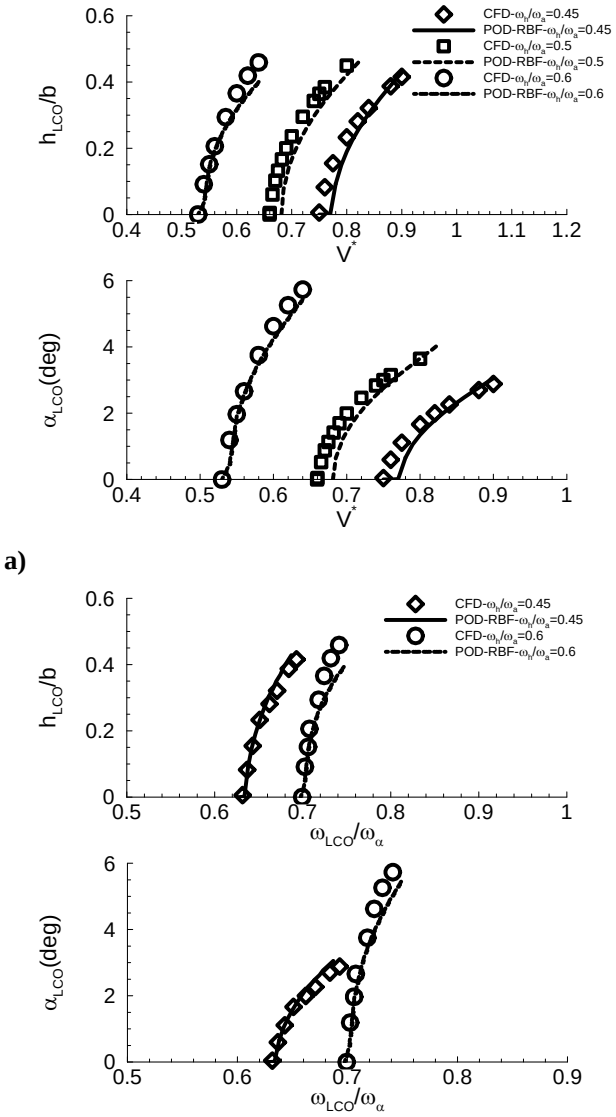

Fig. 13 LCO trends with different uncoupled natural frequency ratios: a) Velocity trend, b) Frequency trend.

After a standard aeroelastic case is studied, the LCO trends after the uncoupled natural frequency ratio ω_h / ω_α changes are then focused. As is shown in Fig. 13, LCO behaviors are influenced by the relative value of each DOF's uncoupled natural frequency. Results demonstrate that the nonlinear ROM is in accordance with physical analysis, and keeps reasonable accuracy on LCO trends.

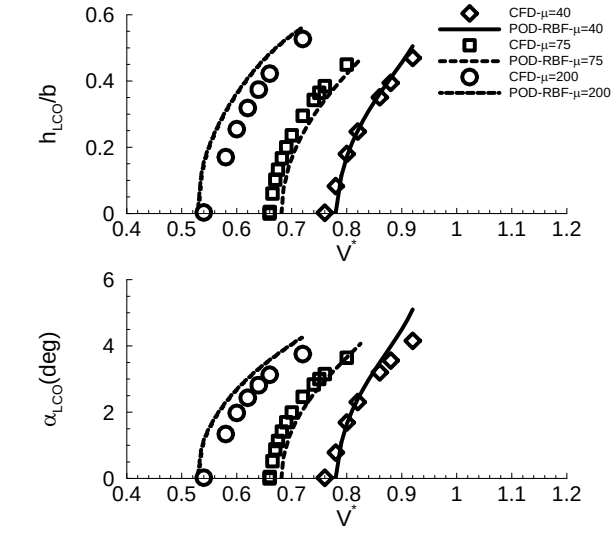

a)

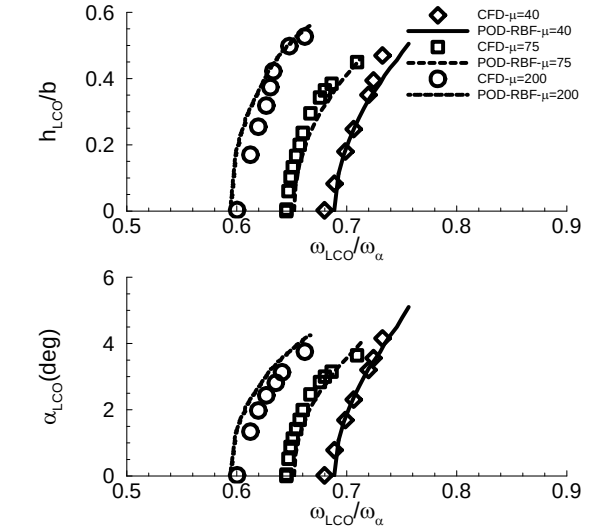

b)

Fig. 14 LCO trends with different uncoupled natural frequency ratios: a) Velocity trend, b) Frequency trend.

In Fig. 14, different LCO trends are noticed when the mass ratio changes. From Fig. 14, a higher mass ratio leads to smaller bifurcation velocity and frequency. This phenomenon can be explained by changes of reduced frequency due to varying mass ratio. The nonlinear ROM based on the proposed POD-RBF network shows accurate LCO trends compared with those of CFD simulations.

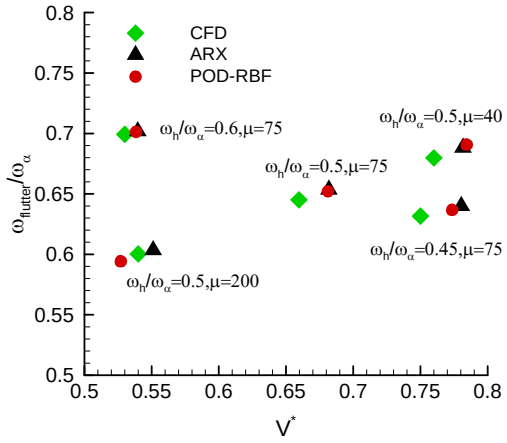

Fig. 15 Comparison of bifurcation point predicted by the proposed ROM, linear ARX model and CFD simulations.

Our study later focuses on flutter characteristics. By using linear ARX model, the flutter reduced velocity and frequency are predicted with acceptable accuracy [6-7]. In this study, ARX model is trained by the validation case shown in Fig. 1b. Fig. 15 demonstrates flutter characteristics of the above-mentioned five structural parameters, given by ARX model, the POD-RBF network and CFD method. Although small deviations (within 5%) with CFD simulations are noticed, the nonlinear ROM exhibits good agreement with linear ROM. This indicates that both the linear and nonlinear dynamics are effectively captured by the POD-RBF model.

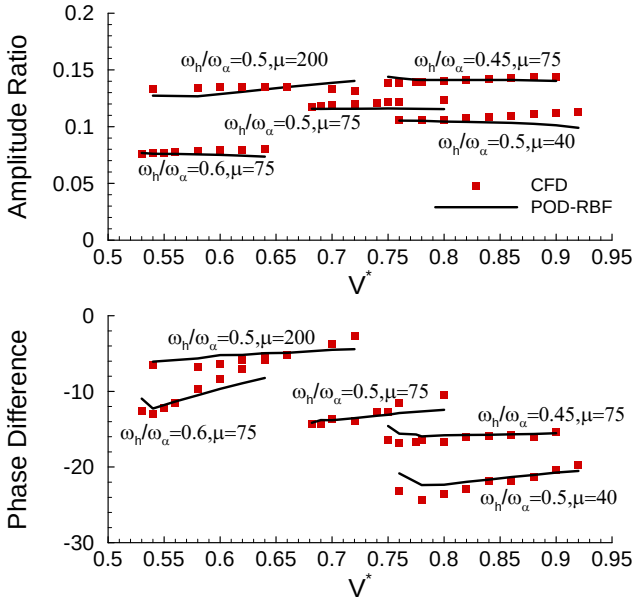

Fig. 16 Amplitude ratio and phase difference of plunging and pitching motions.

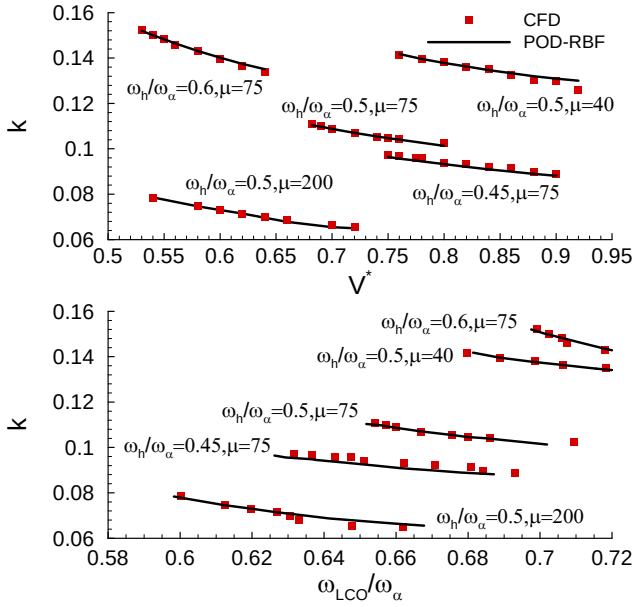

Fig. 17 Trends of LCO frequency at different structural parameters.

For a comprehensive evaluation of the generalization capability, Figs. 16-17 are provided. The amplitude ratio is defined as $h_{LCO}/(b\alpha_{LCO})$, and the phase difference is calculated from the phase difference of first-order Fourier series in plunging and pitching responses. The comparison of ROM and CFD simulations still indicates a close match on the trend of LCO characteristics in the frequency domain. Although reduced frequency trends in Fig. 17 are nearly linear, the POD-RBF network maintains a high accuracy with CFD method.

At last, the time reduction of using the proposed ROM is analyzed. During the modeling process, iterations in seeking for the best width matrix costs 20 minutes at most and each model training is finished within 10 seconds. Calculations of training and validation cases consume a 5-hour computational time (4000 points). Time cost in obtaining a stable limit cycle is a case-by-case problem. Fig 18a shows that 30 cycles are enough at large reduced velocity, but when the reduced velocity is close to bifurcation point, it becomes hard in LCO convergence, as is illustrated in Fig.18b (more than 400 cycles). For a rough estimation, we assume 6 h for each LCO calculation (about 100 cycles). For the nonlinear POD-RBF network, 10 seconds are enough for over 500 cycles. From the overall time

cost comparison in Table. 2, ROM only consumes about 2% of the CFD calculating time.

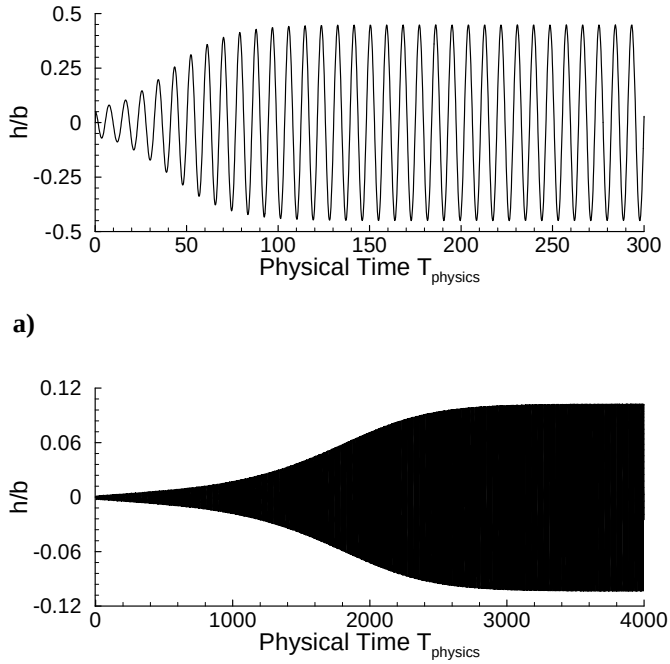

Fig. 18 Typical LCO responses: a) $V^* = 0.8$**, b)** $V^* = 0.67$**.**

Table 2 Comparison between the time cost of direct CFD and the POD-RBF network

Method	Time Cost	Total Time
Direct CFD Simulations	1) Time cost for each case is about 8 h; 2) there are 12 cases for standard condition, and 30 more cases for the conditions considering variations of structural parameters.	T_{CFD}=6×(12+30) h=252h
Nonlinear POD-RBF network	1) Modeling by the POD-RBF network costs 20 min in seeking for width matrix and another 10 s for the final training; 2) Time cost of each LCO response is 10 s; 3) CFD simulations of training and validation case cost 5 h.	$T_{POD\text{-}RBF}$=10s+20min+(12+30) ×10s+5h=5.453h

Ⅴ. Conclusions

A novel RRBF neural network based on POD method is developed in this Note. POD for center selection, PSO and a validation case for width determination and SVD for weight calculations are all utilized for model training. Compared with the previous RRBF neural network model, the POD-RBF network shows high accuracy in simulating aerodynamic responses of a NACA64A010 airfoil, as well as LCO predictions of a standard condition. Furthermore, the LCO trends under different structural parameters are simulated with acceptable accuracy. The comparisons of flutter characteristics illustrate

that the nonlinear ROM contains both dynamically linear and nonlinear characteristics. The computational efficiency of the POD-RBF network is improved by about two orders of magnitude compared with that of the direct CFD method. In the future, applications in more complicated aeroelastic analysis (e.g., a 3D wing or an aircraft) and in different flow conditions (e.g., Mach number) will be considered.

Acknowledgement

This work was supported by the National Natural Science Foundation of China (No. 11572252), Program for New Century Excellent Talents in University (No.NCET-13-0478), and the Seed Foundation of Innovation and Creation for Graduate Students in Northwestern Polytechnical University (No. Z2016002).

Reference

[1] Dowell, E., Edwards, J., and Strganac, T., "Nonlinear Aeroelasticity," *Journal of Aircraft*, Vol. 40, No. 5, 2003, pp. 857-874. doi: 10.2514/2.6876

[2] Zhang, W., Gao, C., Liu, Y., Ye, Z., and Jiang, Y., "The Interaction Between Flutter and Buffet in Transonic Flow," *Nonlinear Dynamics*, Vol. 82, No. 4, 2015, pp. 1851-1865. doi: 10.1007/s11071-015-2282-z

[3] Gao, C., Zhang, W., Liu, Y., Ye, Z., and Jiang, Y., "Numerical Study on the Correlation of Transonic Single-Degree-of-Freedom Flutter and Buffet," *Science China Physics, Mechanics & Astronomy*, Vol. 58, No. 8, 2015, pp. 084701. doi: 10.1007/s11433-015-5683-6

[4] Lucia, D.J., Beran, P.S., and Silva, W.A., "Reduced-Order Modeling: New Approaches for Computational Physics," *Progress in Aerospace Sciences*, Vol. 40, No. 1, 2004, pp. 51–117. doi:10.1016/j.paerosci.2003.12.001

[5] Willcox, K., and Peraire, J., "Balanced Model Reduction via the Proper Orthogonal Decomposition," *AIAA Journal*, Vol. 40, No. 11, 2002, pp. 2323–2330. doi: 10.2514/2.1570

[6] Zhang, W., and Ye, Z., "Reduced-Order-Model-Based Flutter Analysis at High Angle of Attack," *Journal of Aircraft*, Vol. 44, No. 6, 2007, pp. 2086–2089. doi:10.2514/1.32285

[7] Zhang, W., Ye, Z., and Zhang, C., "Aeroservoelastic Analysis for Transonic Missile Based on Computational Fluid Dynamics," *Journal of Aircraft*, Vol. 46, No. 6, 2009, pp. 2178–2183. doi:10.2514/1.45249

[8] Zhang, W., Wang, B., Ye, Z., and Quan, J., "Efficient Method for Limit Cycle Flutter Analysis Based on Nonlinear Aerodynamic Reduced-Order Models," *AIAA Journal*, Vol. 50, No. 5, 2012, pp. 1019–1028. doi:10.2514/1.J050581

[9] Mannarino, A., and Mantegazza, P., "Nonlinear Aeroelastic Reduced Order Modeling by

Recurrent Neural Networks," *Journal of Fluids and Structures*, Vol. 48, July 2014, pp. 103–121. doi:10.1016/j.jfluidstructs.2014.02.016

[10] Kou, J., Zhang, W., and Ye, Z., "Dynamic nonlinear aerodynamics modeling method based on layered model", *Acta Aeronautica et Astronautica Sinica*, Vol. 36, No. 12, 2015, pp. 3785-3797.

[11] Lindhorst, K., Haupt, M. C., and Horst, P., "Efficient Surrogate Modelling of Nonlinear Aerodynamics in Aerostructural Coupling Schemes," *AIAA Journal*, Vol. 52, No. 9, 2014, pp. 1952–1966. doi:10.2514/1.J052725

[12] He, S., Yang, Z., and Gu, Y., "Transonic Limit Cycle Oscillation Analysis Using Aerodynamic Describing Functions and Superposition Principle," *AIAA Journal*, Vol. 52, No. 97, 2014, pp. 1393-1403. doi: 10.2514/1.J052559

[13] Balajewicz, M., and Dowell, E., "Reduced-Order Modeling of Flutter and Limit-Cycle Oscillations Using the SparseVolterra Series," *Journal of Aircraft*, Vol. 49, No. 6, 2012, pp. 1803–1812. doi:10.2514/1.C031637

[14] Kou, J., and Zhang, W., "An Approach to Enhance the Generalization Capability of Nonlinear Aerodynamic Reduced-Order Models," *Aerospace Science and Technology* Vol. 49, No. 1, 2016, pp. 197–208. doi:10.1016/j.ast.2015.12.006

[15] Zhang, W., Guo, X., Wang, C., and Wu, C., "A POD-Based Center Selection for RBF Neural Network in Time Series Prediction Problems," *Adaptive and Natural Computing Algorithms*, Vol. 4432, Lecture Notes in Computer Science, edited by Beliczynski, B., Dzielinski, A., Iwanowski, M., and Ribeiro, B., Springer, Berlin, 2007, pp. 189-198.

[16] Moody, J., and Darken, C.J., "Fast Learning in Network of Locally-Tuned Processing Units," *Neural Computation*, Vol. 1, No. 2, 1989, pp. 281-294. doi: 10.1162/neco.1989.1.2.281

[17] JIANG, Y., "Numerical Solution of Navier–Stokes Equations on Generalized Mesh and Its Applications," Ph.D. Dissertation, Northwestern Polytechnical Univ., Xi'an, China, 2013.

[18] De Boer, A., Van Der Schoot, M.S., and Bijl, H., "Mesh Deformation Based on Radial Basis Function Interpolation," *Computers & Structures*, Vol. 85, Nos. 11-14, June-July 2007, pp. 784-795. doi:10.1016/j.compstruc.2007.01.013

[19] Zhang, W., Jiang, Y., and Ye, Z., "Two Better Loosely Coupled Solution Algorithms of CFD Based Aeroelastic Simulation," *Engineering Applications of Computational Fluid Mechanics*, Vol. 1, No. 4, 2007, pp. 253–262.

[20] Thomas, J. P., Dowell, E. H., and Hall, K. C., "Nonlinear Inviscid Aerodynamic Effects on Transonic Divergence, Flutter, and Limit-Cycle Oscillations," *AIAA Journal*, Vol. 40, No. 4, 2002, pp. 638–646. doi:10.2514/2.1720